MECSOL 2022 - Proceedings of the 8th International Symposium on Solid Mechanics
M.L. Bittencourt, J. Labaki, L.C.M. Vieira Jr. and E. Mesquita (Editors), Campinas SP, Brazil, October 17th to 19th, 2022

Theory and Application of the Applied Element Method in Linear Elastic Regime

César Eduardo Petersen[1] and Ricardo Pieralisi[2]

[1] Postgraduate Program in Civil Engineering (PPGEC), Federal University of Paraná - UFPR, Curitiba, PR, Brazil.

[2] Civil Engineering Studies Center (CESEC), Postgraduate Program in Civil Engineering (PPGEC), Federal University of Paraná - UFPR, Curitiba, PR, Brazil.

Abstract: The Applied Element Method (AEM) divides a structure into smaller rigid elements connected by a series of normal and tangential springs pairs spread along the element edge. It combines the advantages of both finite and discrete element methods (FEM and DEM, respectively), allowing accurate results from small displacements to large deformations. In AEM, each element has 3 degrees of freedom (DoFs). The body assembly stiffness matrix is a sum of every spring pair stiffness. The Poisson effect is also modeled without the addition of extra DoFs, by considering the effect of neighboring elements on the assembly. Strain and stress are calculated from relative displacements of the springs, and the stress in each element is the average of the stresses in its connected springs. In this work, the basic linear-elastic formulation of the method was implemented on C++. A cantilever beam with applied load and a fixed beam with distributed load were analyzed. The models were compared with theoretical models as well as traditional FEM models on ANSYS 2021 R2 educational version with equivalent element sizes. A mesh sensitivity analysis was also done, with the model successfully converging with elements about 1/40 of the smallest dimension.

Keywords: Applied element method, Numerical Methods, Structural Analysis, Computational Mechanics

INTRODUCTION

According to Tagel-Din (1998), numerical methods can be classified into two categories: Models based on equations for continuous materials, such as the Finite Element Method (FEM), and methods that use discrete element techniques such as the Discrete Element Method (DEM). Each type of model is suitable for a scale of displacements, FEM operates in the small displacement regime, allowing to determine whether or not a structure will fail. While discrete models work in the regime of large displacements, allowing to determine how a structure fails, but without the accuracy required in the small displacements to determine the critical load.

Meguro and Tagel-Din (2000) then proposed the Applied Elements Method, AEM, taking advantage of both continuous and discrete approaches. The method divides the body into rigid elements with 3 Degrees of Freedom (DoFs) for horizontal and vertical displacement as well as rotation, connected by pairs of springs spread along its connections. The spring pairs are for normal and tangential strains, and their stiffness are derived from the material properties such as Youngs' modulus and Poisson ratio. This formulation also allows for a simplified representation of reinforcement in the structure by merely adding a spring with equivalent steel stiffness at the appropriate positions. The strains and stresses for the body are finally obtained from the relative spring's displacements.

Meguro and Tagel-Din (2000) also incorporated the Poisson effect without extra DoFs in the formulation of the method, generally not considered in rigid body models. With the AEM, they were also able to accurately simulate fractures, collapse, separation of elements and large deformations. In particular, according to Gohel, Patel e Joshi (2013), the fracture model used in the method allows representing the propagation of fractures without the need for an initial fissure.

The method has been successfully applied in the analysis of progressive collapse by other authors such as Domaneschi *et al.* (2020) and Christy, Nagarajan and Pillai (2021) for example, where they also highlight the efficiency of the method in relation to the traditional FEM. The literature of the method, however, is still scarce, particularly in the Portuguese language, and especially in Brazil, with only a single dissertation (MARTINS, 2019) that briefly discusses the method, but does not perform a simulation due to the difficulty of acquiring the only available commercial *software*, *Extreme Loading® for Strucures*. The method, therefore, has a certain aspect of novelty in Brazil. This *software* limitation is also a factor to consider, with very few studies in this regard, for example, Shakeri and Bargi (2015) who programmed a routine in FORTRAN to use the AEM, evidencing the need for further development in the area.

APPLIED ELEMENT METHOD

According to Meguro and Tagel-Din (2000), in AEM, the structure is modeled by a set of small rigid elements with three degrees of freedom (horizontal and vertical displacements, and rotation), and can be considered as material points, connected by pairs of normal and tangential springs distributed along the edges of the elements. Although the elements do not deform, their assembly is deformable. In the initial pre-processing stage, all the parameters necessary for the construction of the model are configured (such as Material properties, the Geometry and Boundary Conditions), resulting in a mesh of elements and connections. The connections are iterated generating all pairs of normal and tangential springs according to a constitutive law. Each spring connecting a pair of elements has a local stiffness matrix associated with it, and then the global stiffness matrix (K_G) is determined by adding the matrices of all the springs in all of the elements of the model. With a vector of applied forces (F), displacements (Δ) can be determined by the model's governing equation, Eq. (1) according to Meguro e Tagel-Din (2000, p. 34). The Poisson effect is accounted for in the global stiffness matrix by analyzing all neighboring elements. With solved displacements and forces, strains and stresses can be determined for the elements.

$$[K_G]\{\Delta\} = \{F\} \tag{1}$$

The implementation details of each stage are further explained.

Pre-processing stage

Preprocessing is the initial step in building a model. In it, the definitions of the materials used, the geometry of the model and the boundary conditions are defined. An example of a bi-supported beam model of height (H) and Length (L), with distributed loads (q) and concentrated (F), and rebars, is presented on Figure 1. For the material, a linear-elastic isotropic material with Young's modulus (E) and Poisson ratio (v) as parameters. Shear modulus (G) can then be derived from both.

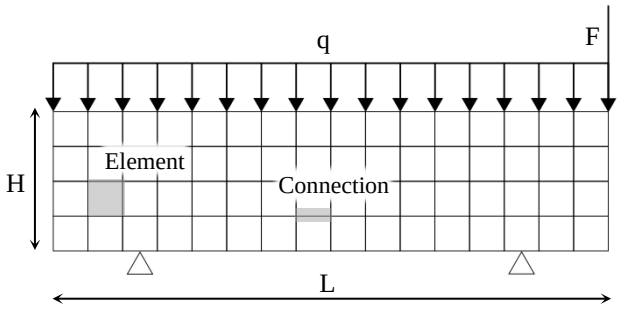

Figure 1 – Element mesh.

Constitutive laws are used to calculate the spring's stiffness. Meguro and Tagel-Din (2000) use simple Elastic-Linear law to calculate. From Hooke's law for springs and for continuous media, Eq. (2) and Eq. (3), respectively, it can be derived the basis formulation for the spring's normal stiffness, Eq. (4).

$$F = k \cdot \Delta x \tag{2}$$

$$\sigma = {}^{F}/_{A} = E \cdot \varepsilon \tag{3}$$

$$k = {}^{EA}/_{x_0} \tag{4}$$

As illustrated by Figure 2, considering the undeformed length (x_0) as the distance between centers (a), the area (A) as the cross section of the spring's influence zone for an element with thickness (T) and distance (d) between the equally spaced springs, and, analogously, using the Shear module for tangential stiffness, one can deduce Eqs. (5) for normal (Kn) and tangential stiffness (Ks). If the elements have different materials or thickness, the average stiffness between the two elements is taken. For the case of rebar's springs, the area is the bar's own cross-section area and steel Young and Shear modulus.

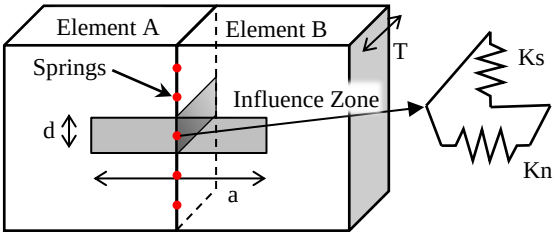

Figure 2 – Springs influence zone.

$$\begin{cases} Kn = \frac{ETd}{a} \\ Ks = \frac{GTd}{a} \end{cases} \tag{5}$$

According to Meguro and Tagel-Din (2000), the rotational stiffness (K_r) of an element with height (h), thickness (T) and Young's modulus (E) is given by Eq. (6). The same rotational stiffness can be discretized for n number of springs equally spaced, as Eq. (7). Meguro and Tagel-Din (2000) note that 10 springs per connections reduces the error rate for the rotational stiffness to less than 1%, while still maintaining a low computational cost. A parametric analysis by the authors also concludes that reducing the elements size contributes greatly to the results precision, while increasing the number of springs brings no meaningful results.

$$K_r = \int_{-h/2}^{h/2} \frac{ET}{h} z^2 dz = \frac{ETh^2}{12} \tag{6}$$

$$K_r = \frac{ETh^2}{4n^3} \sum_{i=1}^{n} (i - 0{,}5)^2 \tag{7}$$

Processing Stage

With all the springs distributed along the model's connections, the stiffness matrix can be assembled. The method iterates all the springs calculating their local stiffness matrix, rotating it to the global coordinates and summing it to the global stiffness matrix. The local stiffness matrix for a pair of normal e tangential springs, representing the 3 DoFs for the left element and 3 DoFs for the right element, is given by Eq. (8), where x_i and y_i are the distances in the element's local coordinates, as shown in Figure 3a. The unit vector ***e***, pointing from the left-side element's center to the other, also on Figure 3a, is responsible for rotating between the local and global coordinates.

$$\begin{bmatrix} Kn & 0 & -Kn \cdot y_1 & -Kn & 0 & Kn \cdot y_2 \\ 0 & Ks & Ks \cdot x_1 & 0 & -Ks & Ks \cdot x_2 \\ -Kn \cdot y_1 & Ks \cdot x_1 & Kn \cdot y_1^2 + Ks \cdot x_1^2 & -Kn \cdot y_1 & -Ks \cdot x_1 & -Kn \cdot y_1 \cdot y_2 + Ks \cdot x_1 \cdot x_2 \\ -Kn & 0 & -Kn \cdot y_1 & Kn & 0 & -Kn \cdot y_2 \\ 0 & -Ks & -Ks \cdot x_1 & 0 & Ks & -Ks \cdot x_2 \\ Kn \cdot y_2 & Ks \cdot x_2 & -Kn \cdot y_1 \cdot y_2 + Ks \cdot x_1 \cdot x_2 & -Kn \cdot y_2 & -Ks \cdot x_2 & Kn \cdot y_2^2 + Ks \cdot x_2^2 \end{bmatrix} \tag{8}$$

As for the Poisson effect, Meguro and Tagel-Din (1998) adopted an approach to represent the Poisson effect without relying on extra DoFs. The authors correlate the stiffness matrix of the element with the edges of adjacent elements through continuity factors. They determine the link between an element and its surrounding neighbors, adopting the value +1 when there is a neighboring element, and zero in its absence, allowing a generalization of the stiffness matrix.

According to Meguro and Tagel-Din (2000), for each degree of freedom of the elements, additional terms in the stiffness matrix are obtained by assuming a displacement on the direction of the DoF and calculating the deformation imposed on the centroid of the elements, and considering the transmitted forces and moments to the neighboring elements from element *i*, p_i and m_i, respectively, given by Eqs. (9) and (10).

$$p_i = \frac{\nu \cdot E_i \cdot t_i}{4(1-\nu^2)} \tag{9}$$

$$m_i = \frac{\nu \cdot E_i \cdot t_i}{4(1-\nu^2)} \cdot \frac{D}{4} \tag{10}$$

The model governing equation can be solved just like in FEM models, the stiffness matrix is reorganized into submatrices for the free and fixed DoFs, as well as the force and displacement vectors. The free applied forces and prescribed displacements on the supports are known, while the reaction fixed forces and free displacements are the unknowns.

The last step is to determine the strains and stresses of the elements. The steps adopted by Meguro and Tagel-Din (2000) consists of:

1. For each spring, calculate normal and tangential deformations from the relative displacement of the springs (Δx and Δy) with $\varepsilon = \Delta/D$, where D is the size of the element;
2. For each element, calculate the mean deformations $\bar{\varepsilon}$ on directions x and y;
3. Correct the springs deformation with $\varepsilon'_x = \varepsilon_x + \nu\bar{\varepsilon_y}$ e $\varepsilon'_y = \varepsilon_y + \nu\bar{\varepsilon_x}$, where ν is the Poisson ratio;
4. Calculate stresses $\sigma = E\varepsilon'/(1-\nu^2)$.

Figure 3b demonstrates this procedure. From the local configuration of the undeformed element, the relative displacements of the springs are obtained (closed arrow vectors, connecting both elements), the open arrow vector represents the displacement of the element. Δy represents a tangential deformation and Δx a normal deformation. These

deformations are transformed to the global configuration to make up the average deformation of the element. As a deformation in the global *x* direction will not contribute to the deformation *y* of the element, and vice versa, a weighted average was adopted to calculate the average deformation of the element. For a deformation vector $\boldsymbol{\varepsilon} = \{\varepsilon_x, \varepsilon_y, \tau_{xy}\}$, a weight vector $\boldsymbol{p} = \{\cos^2\theta, \text{sen}^2\theta, 1\}$ was adopted, where θ represents the direction between the centers of the undeformed elements, also represented by the aforementioned ***e*** unit vector. With the corrected deformations, the stresses of the springs can be calculated.

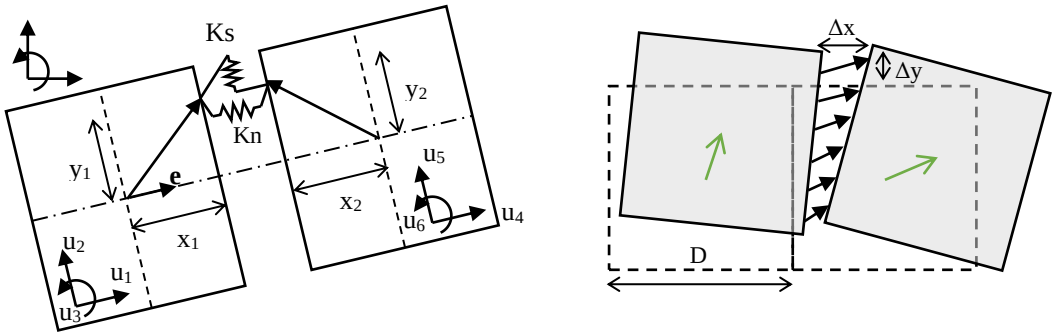

(a) Spring connecting a pair of elements. (b) Stress-Strain calculation on springs.

Figure 3 – Connection scheme and stress-strain calculation.

STATE OF THE ART

Gohel, Patel and Joshi (2013) they performed a static analysis of a frame using the Applied Elements Method, comparing it with an analysis using the Finite Element Method. According to the authors, one of the main advantages of the method is to allow the propagation of cracks in any location of the model, without the need for an initial crack. A two-column frame and a beam with lateral load applied to the top left corner under 4 element size settings (300, 200, 150 e 120mm) and 5 springs number (1 ,3, 5, 7 e 10 springs on each connection) were simulated. The authors observed that the accuracy of the results increased with the use of smaller elements, and also with fewer spring connections than suggested by Meguro and Tagel-Din (2000).

Christy, Nagarajan and Pillai (2019) developed a thin plate element for the AEM that allows working with out-of-plane transverse loads. The authors adapted a three-dimensional element by simplifying it for the plane stress and plane strain cases, considering only 3 degrees of freedom, the rotations in the x and y axes, and displacement on the z axis, with the corresponding stiffness matrix to the springs, one normal, and two tangential. Christy, Nagarajan and Pillai (2019) also simplify the stiffness matrix, considering infinite springs along the section and integrating the matrix, obtaining a new one that represents the entire section and can be used directly, instead of adding the matrices of each spring individually. The last modification proposed by the authors refers to the Poisson effect, which plays a fundamental role in the behavior of plates. A unit displacement in the z direction generates no normal effort in the springs, generating no Poisson effect, the rotations in x and y, however, generate. The authors proceed with a detailed deduction of these effects, applying unitary displacements and calculating normal stresses in the elements. The elements are divided into 4 parts by their center, and the forces and moments of each quarter of the element are calculated, thereby determining additional stiffnesses to be added to neighboring elements. Christy, Nagarajan and Pillai (2019) performed both a static and dynamic analysis on a 1,2x1,2m plate and 30mm thickness, with 100 springs per connection, and the method was able to accurately predict displacements, stresses, moments, torsion and shear forces.

Christy, Nagarajan and Pillai (2021) also draw attention to the small amount of literature, especially discussing the stiffness matrix. The authors deduce in detail the matrix for elements in two dimensions and also the matrix for three-dimensional elements and apply the same simplification presented in the previous paragraph: considering infinite springs in a section, integrating and obtaining a single new matrix. According to the authors, this technique, besides simplifying the model, also increases its precision. All formulas for calculating strains, stresses, bending moments and shear force are also deduced. The method was verified by simulating models of cantilever beams with rectangular section, with circular section, and a frame, all of which accurately predicted the results, in some cases even better than the finite element method.

An important area of study involving the Applied Elements Method is the progressive collapse of structures, due to the ability to simulate all the behavior of a structure from small displacements to separation. El-desoqi, Ehab and Salem (2020) carried two simulations in framed structures, with and without the contribution of the slab to the stiffness of the structure, under its own weight. Several column removal scenarios were simulated, with different beam lengths and, as expected, the structures with the slab consideration resisted more.

Domaneschi *et al.* (2020) carried out an analysis of the collapse of the *Polcevera* viaduct in Italy in 2018. The entire central structure of the collapsed viaduct was modeled with three-dimensional elements at the highest level of detailing, with all the viaduct reinforcement included, and nonlinear constitutive models for the materials. In all, the model contained 150,000 elements in a time step Δt = 0.001s, with a total computing time of almost 48h. Simulations were

performed removing/degrading various parts of the viaduct until the collapse was reached, thus it was possible to determine the probable cause of the collapse as a degradation in one of the viaduct cables, when approximately 60% of its area was removed. The simulations were compared instant by instant with images and videos provided by the local police and firefighters and indicate that the simulation showed a good agreement with the real collapse mechanism of the structure, at least in the first 5 seconds.

METHODOLOGY

The method was implemented in C++ using an Object-Oriented approach. The *Eigen3* library (GUENNEBAUD; JACOB et al., 2020) was used for the linear algebra needed, and SWIG – *Simplified Wrapper and Interface Generator* (THE SWIG DEVELOPERS, 2020), was also used to integrate code with Python, allowing the assembly of simulations interactively, without the need to re-compile the codebase. As for the post-processing stage, the VTK (SCHROEDER; MARTIN; LORENSEN, 2006) on Legacy ASCII format was used to export the results, such as: displacements and rotation fields, strains, stresses and principal stresses. These files can then be examined on *ParaView* (AYACHIT, 2015).

Initially, three simple models were analyzed through the AEM, and compared with equivalent models on traditional FEM with *ANSYS 2021 R2* educational version, using linear 4-node rectangular elements. Besides, a mesh sensitivity analysis will be performed, varying the size of the elements.

The first model is a prismatic body with base 20x20cm and height 36cm, under an axial load as illustrated on Figure 4a, the body is simply supported on its base and has a force P = +10kN distributed on its upper face. The material has a Young's modulus E = 26GPa, and a Poisson ratio ν = 0.2. The model was meant to be compared with the one from Meguro and Tagel-Din (2000), however, the current implementation of the method only allowed to mimic the rigid plates on the top and bottom by applying an equivalent distributed load q = P/0.20 = 50kN/m on the top row of elements, and fixing the bottom row, not considering the effects of sliding with and without friction.

Cantilever beams with both distributed and applied loads, as shown in Figure 4b, were simulated. The beams have a length L = 2m, cross-section of 20x40cm, with moment of inertia I = $1.067 \cdot 10^{-3} m^4$, Young's modulus E = 25GPa and Poisson ration ν = 0.2, distributed load q = 20kN/m and applied load P = 50kN. For the applied load model, it's important to consider that the loads are applied on the element's centroid, thus, a load on the top left corner also carries an associated moment from the element corner to its center.

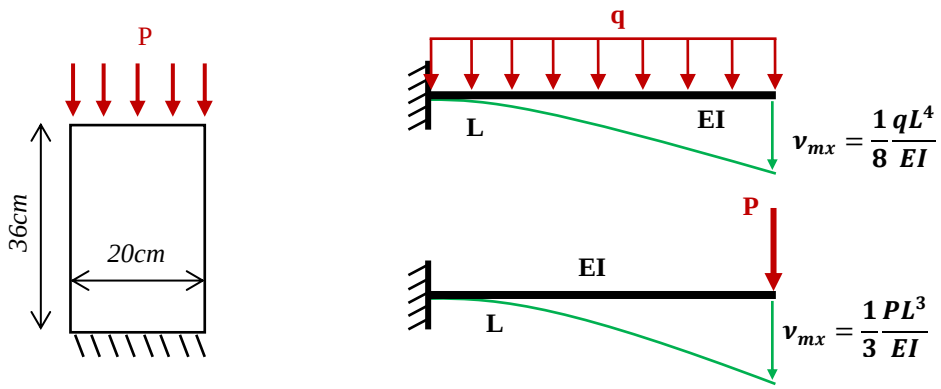

(a) Axial model (b) Beam models

Figure 4 – Simulated Models.

RESULTS AND DISCUSSION

The first simulated model was the axial load, with its results listed on Table 1. The theorical error was compared to a displacement of an axial bar δ = PL/EA = $3{,}461 \cdot 10^{-3}$mm, besides the equivalent model on FEM. The vertical displacement was obtained on the middle of the model's top surface.

Table 1 - Axial load model results summary.

Case	Element size (cm)	Number of elements	Vertical Displacement (mm x 10^{-3})	Theorical Error (%)	FEM Displacement (mm x 10^{-3})	FEM Error (%)
1	2.0 x 2.0	180	3.542	+2.34	3.5886	-1.30
2	1.0 x 1.0	720	3.647	+5.37	3.589	+1.62
3	0.5 x 0.5	2880	3.700	+6.91	3.589	+3.09
4	0.4 x 0.4	4500	3.711	+7.22	3.589	+3.40
5	0.25 x 0.25	11520	3.727	+7.69	3.589	+3.85
6	0.2 x 0.2	15000	3.732	+7.83	3.589	+3.98

Figure 5 presents the plotted results for the 3º case, with 0.5x0.5cm elements. The models show a good physical coherence with Meguro and Tagel-Din (2000), although, due to the limitations of the current implementation, it's not possible to correctly simulate the effect of rigid plates on the upper and lower surfaces of the model, resulting on stress concentrations on the corners.

The mesh sensitivity analysis shown on Figure 5e shows a convergence of the maximum displacement value after approximately 3000 elements, with the element size approximately $1/40$ of the model's smallest dimension, in addition to comparing with the results of the equivalent model in FEM, with error below 5%.

(a) Displacement magnitude [m]

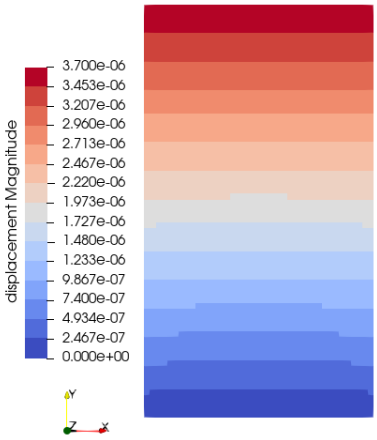

(b) X Stress [kPa]

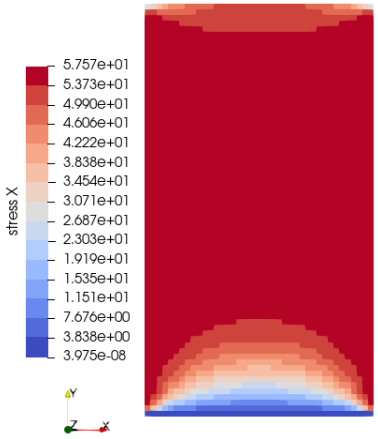

(c) Y Stress [kPa]

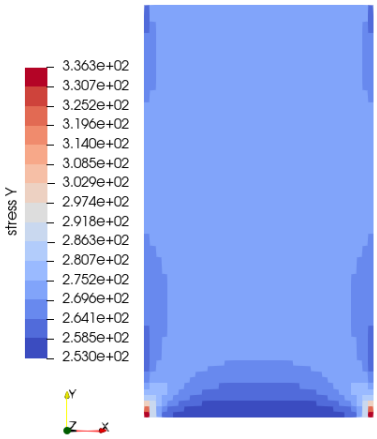

(d) XY Tangential Stress [kPa]

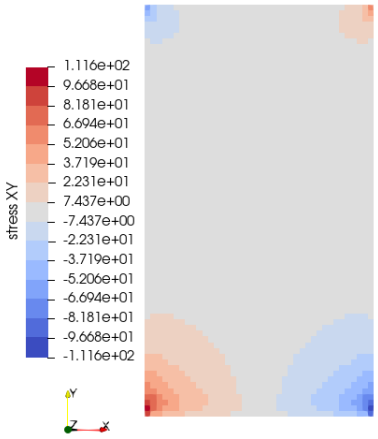

(e) Mesh sensitivity analysis

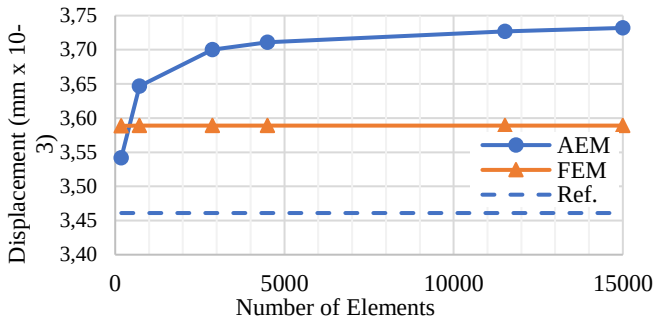

Figure 5 – Axial Model results.

The second simulated model was the cantilever beam with distributed load. The results with vertical displacement from the bottom right corner element and the comparison with the equivalent FEM model are shown on Table 2. As a reference value for the theorical displacement, $\delta = qL^4/8EI = 1.500$mm was adopted. Figure 6(a) to (d) show the displacement field and stresses for the 8º Case model, with the deformed displacement field exaggerated 100 times. Figure

6(b) and (c) comparing the X stress between AEM and FEM show an almost identical behavior. The model also appears to converge after about 4000 elements, as shown in Figure 6(e), and the FEM results are whiting a 5% margin.

Table 2 – Cantilever with distributed load model results.

Case	Element size (cm)	Number of elements	Vertical Displacement (mm)	Theorical Error (%)	FEM Displacement (mm)	FEM Error (%)
1	2.0 x 20.0	200	1.559	+3.93	1.5502	+0.57
2	1.0 x 20.0	400	1.580	+5.33	1.5504	+1.91
3	0.5 x 20.0	800	1.590	+6.00	1.5506	+2.54
4	0.4 x 20.0	1.000	1.592	+6.13	1.5506	+2.67
5	0.4 x 10.0	2000	1.601	+6.73	1.5548	+2.97
6	0.2 x 10.0	4.000	1.605	+7.00	1.5548	+3.23
7	0.2 x 8.0	5.000	1.607	+7.13	1.5556	+3.30
8	0.2 x 4.0	10.000	1.609	+7.27	1.5557	+3.43

(a) Displacement magnitude (exagerated 100x) [m]

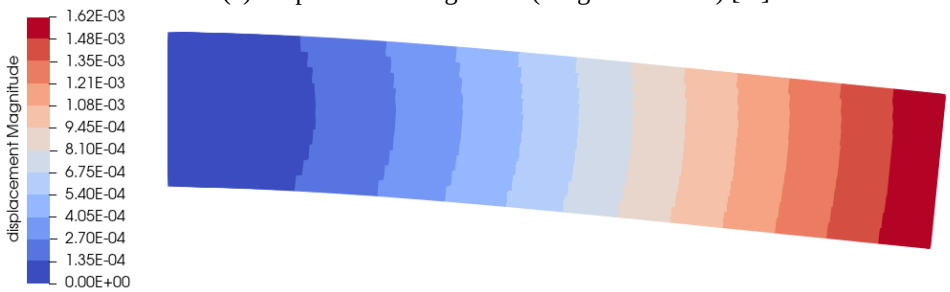

(b) X Stress [kPa]

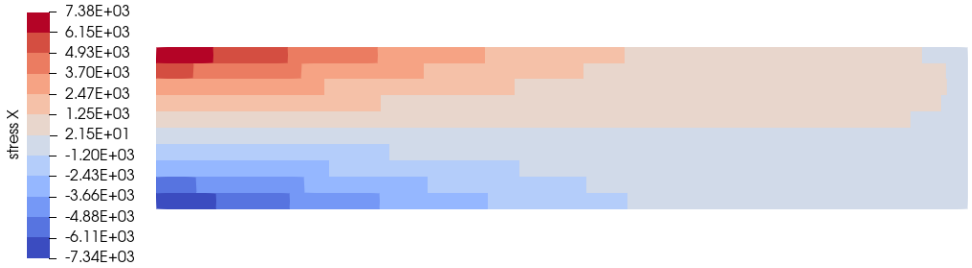

(c) FEM X Stress [Pa]

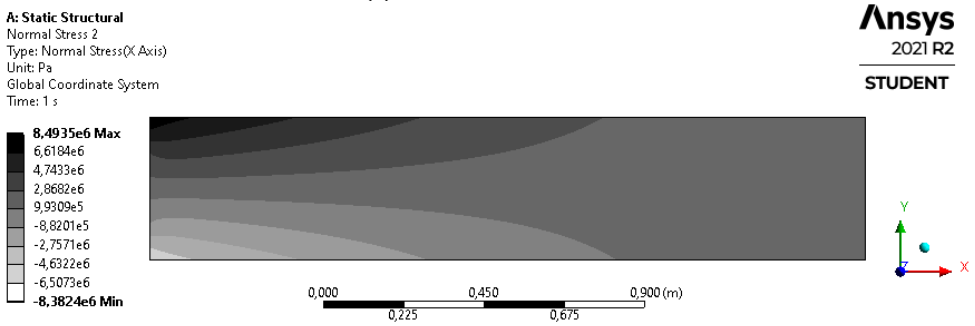

(d) XY Tangential Stress [kPa]

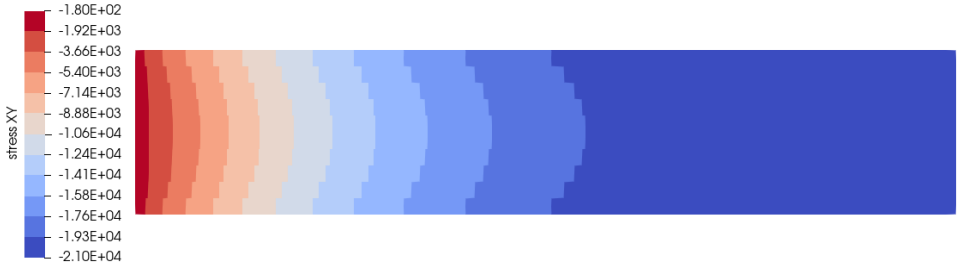

Figure 6 – Cantilever with distributed load Model results. **(Continues on the next page)**

(e) Mesh sensitivity analysis

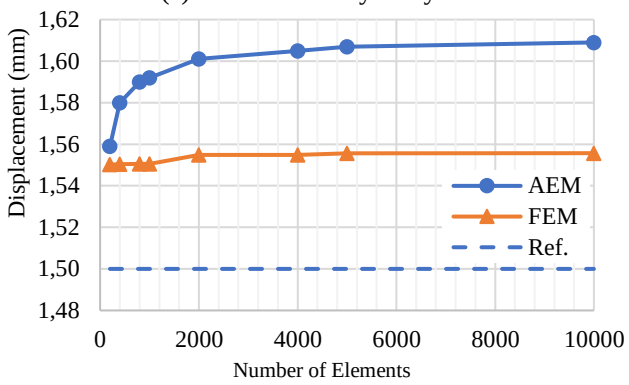

Figure 6 – Cantilever with distributed load Model results.

The cantilever beam with applied load model results with vertical displacement from the bottom right corner element is shown on Table 3, for the theorical reference value, a traditional Euler-Bernoulli beam was adopted, with displacement $\delta = PL^3/3EI = 5.118$mm. Figure 7(a) to (e) show the displacement field and stresses for the 8º Case model, with the deformed displacement field exaggerated 40 times. The comparison between Figure 7(b) and (c) also show a similar behavior between the two methods. Similarly to the previous model, Figure 7(f) also appears to converge after about 4000 elements, with the FEM results whiting a 5% margin, with the FEM results fluctuating though.

Table 3 – Cantilever with applied load model results.

Case	Element size (cm)	Number of elements	Vertical Displacement (mm)	Theorical Error (%)	FEM Displacement (mm)	FEM Error (%)
1	2.0 x 20.0	200	5.138	-0.77	5.1377	+0.01
2	1.0 x 20.0	400	5.194	+0.31	5.1813	+0.25
3	0.5 x 20.0	800	5.223	+0.87	5.2678	-0.85
4	0.4 x 20.0	1.000	5.228	+0.97	5.3110	-1.56
5	0.4 x 10.0	2000	5.247	+1.33	5.1639	+1.61
6	0.2 x 10.0	4.000	5.259	+1.56	5.2174	+0.80
7	0.2 x 8.0	5.000	5.261	+1.60	5.0610	+3.95
8	0.2 x 4.0	10.000	5.264	+1.66	5.1348	+2.52

(a) Displacement magnitude (exagerated 40x) [m]

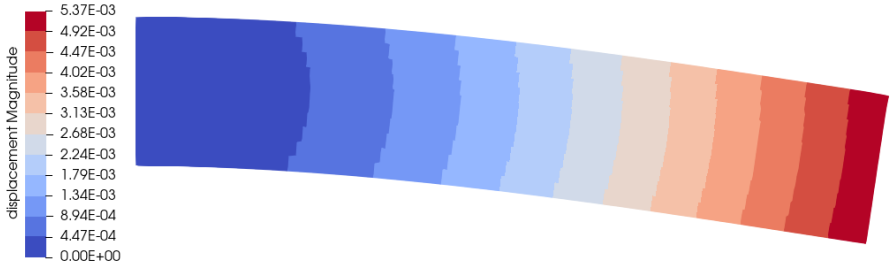

(b) X Stress [kPa]

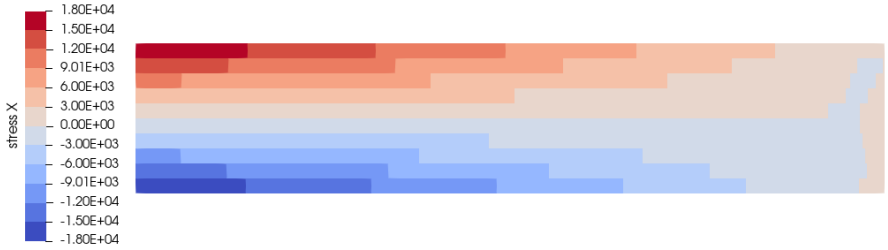

Figure 7 – Cantilever with applied load Model results. (Continues on the next page)

(c) FEM X Stress [Pa]

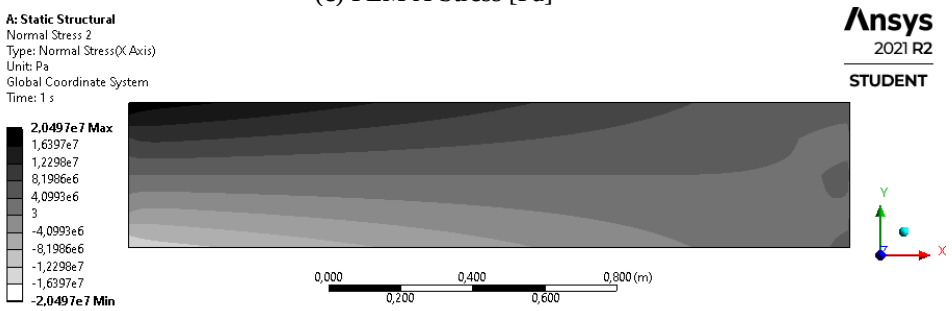

(d) Y Stress [kPa]

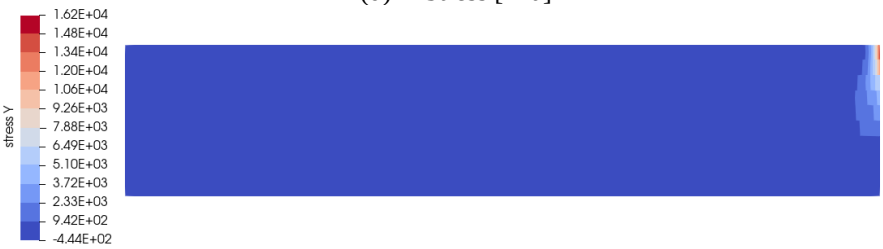

(e) XY Tangential Stress [kPa]

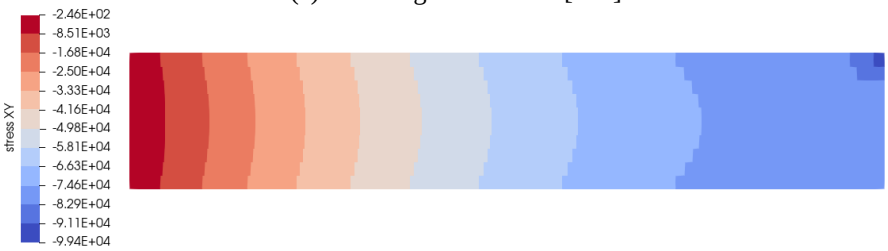

(f) Mesh sensitivity analysis

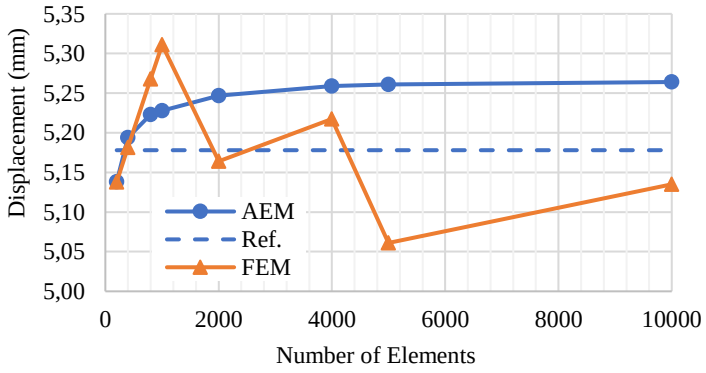

Figure 7 – Cantilever with applied load Model results.

CONCLUSION

This paper applied the Applied Element Method with three models, detailing its main linear-elastic formulation. The method formulation is straightforward, with a single stiffness matrix for its main component: the springs.

The model's results show consistent physical behavior, however it seems more flexible than theorical and equivalent FEM models. The theorical reference values differences are not greater than 8% after convergence of results, while the FEM models differences stay within a 4% margin.

The FEM models, with the exception of the cantilever with a point load, converged with fewer elements and a rougher mesh than AEM. And, although FEM benefits from elements with a "square-ish" aspect-ratio, the cantilever AEM models showed a quicker convergence with the use of rectangular elements. This, however, prevents them from considering the Poisson effect, as it's defined for square elements only. Further studies are needed comparing the effect of the element's aspect ratio on the convergence, as well as extending the Poisson effect formulation for other element shapes.

While its might not be advantageous to use AEM over FEM for simple linear-elastic models, AEM truly shines when it comes to non-linearity, contact problems and concrete reinforcements, as exampled on the literature review, in particular, for the field of progressive collapse of structures. Those, however, were not in the scope of this paper.

ACKNOWLEDGMENTS

The authors thank the Postgraduate Program in Civil Engineering (PPGEC) at the Federal University of Paraná (UFPR). This study was financed in part by the Coordenação de Aperfeiçoamento de Pessoal de Nível Superior - Brasil (CAPES) - Finance Code 001.

REFERENCES

AYACHIT, U., 2015, "The ParaView Guide: A Parallel Visualization Application", Kitware.

CHRISTY, D. L., NAGARAJAN, P. and PILLAI, T. M. M., 2019, "Thin plate element for applied element method", Structures, Vol. 22, pp. 1-12.

CHRISTY, D. L., NAGARAJAN, P. and PILLAI, T. M. M., 2021, "Simplified analysis of structures using applied element method", Songklanakarin Journal of Science and Technology, Vol. 43, No. 1, pp. 133-143.

DOMANESCHI, M., PELLECCHIA, C., DE IULIIS, E., CIMELLARO, G. P., MORGESE, M., KHALIL, A. A. and ANSARI, F., 2020, "Collapse analysis of the Polcevera viaduct by the applied element method", Engineering Structures, Vol. 214, pp. 110659.

EL-DESOQI, M., EHAB, M. and SALEM, H., 2020, "Progressive collapse assessment of precast reinforced concrete beams using applied element method", Case Studies in Construction Materials, Vol. 13, pp. e00456.

GOHEL, V., PATEL, P. V. and JOSHI, D., 2013, "Analysis of Frame using Applied Element Method (AEM)", Procedia Engineering, Vol. 51, pp. 176-183.

GUENNEBAUD, G., JACOB, B. *et al.*, "Eigen v3", http://eigen.tuxfamily.org.

MARTINS, P. H. S., 2019, "Procedimentos e projeto de demolições para edificações em concreto armado", UFSCar, São Carlos.

MEGURO, K. and TAGEL-DIN, H., 1998, "Consideration of Poisson's Ratio Effect in Structural Analysis Using Elements with Three Degrees of Freedom", Bulletin of Earthquake Resistant Structure, IIS, University of Tokyo, No. 31, pp. 41-50.

MEGURO, K. and TAGEL-DIN, H., 2000, "Applied Element Method for Structural Analysis: Theory and Application for Linear Materials", J. Struct. Mech. Earthquake Eng., Vol. 2000, No. 647, pp. 31-45.

SCHROEDER, W., MARTIN, K. and LORENSEN, B., 2006, "The Visualization Toolkit", Kitware.

SHAKERI, A. and BARGI, K., 2015, "Use of Applied Element Method for Structural Analysis", KSCE Journal of Civil Engineering, Vol. 19, No. 5, pp. 1375-1384.

TAGEL-DIN, H., 1998, "A new efficient method for nonlinear, large deformation and collapse analysis of structures", Universidade de Tóquio, Tóquio.

THE SWIG DEVELOPERS, "SWIG - Simplified Wrapper and Interface Generator", http://www.swig.org/.

TIMOSHENKO, S. and GOODIER, J. N., 1951, "Theory of Elasticity", McGraw-Hill Book Company, New York.

RESPONSIBILITY NOTICE

The authors are the only parties responsible for the printed material included in this paper.